

Effect of manganese on the speciation of neptunium(V) on manganese doped magnetites

Sumit Kumar^{a,b,*}, Jörg Rothe^b, Nicolas Finck^b, Tonya Vitova^b, Kathy Dardenne^b, Aaron Beck^b, Dieter Schild^b, Horst Geckeis^b

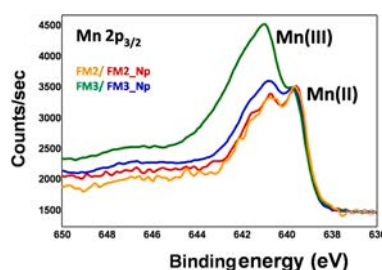
^a Radioanalytical Chemistry Division, Bhabha Atomic Research Centre, Trombay, Mumbai 400085, India

^b Karlsruhe Institute of Technology, Institute for Nuclear Waste Disposal, D-76021 Karlsruhe, Germany

HIGHLIGHTS

- Single phase manganese-doped (3–12 wt%) magnetites were synthesized.
- Neptunium(V) interaction with Mn-doped magnetites in neutral pH condition.
- HR-XANES confirmed single speciation of Np on undoped and doped magnetites.
- Mn-O sites participates through Fe(II)/Mn(III) redox couple in reducing Np(V).

GRAPHICAL ABSTRACT



ARTICLE INFO

Keywords:

Neptunium(V)
Manganese doping
Magnetite
HR-XANES
Redox process

ABSTRACT

Speciation and fate of radionuclides in environment are strongly dependent on their interaction with various mineral surfaces. Presence of impurity atoms in minerals modifies these interactions. ²³⁷Np, a long-lived component of nuclear high-level waste, is highly mobile in environment as neptunyl (NpO₂⁺) cation. Role of impurities in defining its interaction with mineral surfaces present in natural and engineered systems is yet to be completely understood. Manganese is a ubiquitous impurity present in naturally occurring iron corrosion product, magnetite. Here, a series of manganese (Mn)-doped magnetites (FM) was synthesized and the evolution of solid-sorbed speciation of Np(V) was investigated as a function of Mn doping (3–11 wt%) in near neutral pH condition. Combining Mn K-edge and Np L₃-edge X-ray absorption fine structure spectra with Np M₅-edge high energy-resolution X-ray absorption near-edge structure spectra, we found nanoparticulate Np^{IV}O₂ solid as the single speciation of Np sorbed on both doped and undoped magnetites. Without changing the surface speciation of Np, Mn-O sites did show preference for sorbing Np(V) vis-à-vis Fe-O sites. Mn participates through Fe(II)/Mn(III) redox couple in reducing sorbed Np(V). Its participation, however, becomes significant only when the doped-magnetite contains a critical minimum concentration (> 6 wt%) of Mn. This study highlights the significant role of impurity atom wherein it interacts with sorbing species through redox process.

Abbreviations: XAFS, X-ray absorption fine structure spectroscopy; HR-XANES, High-energy resolution X-ray absorption near edge Spectroscopy; FM, Magnetite; HLW, High level radioactive waste; FCC, face centered cubic; ICP-MS, Inductively coupled plasma-mass spectrometry; XRD, X-ray diffraction; SEM, Scanning electron microscopy; XPS, X-ray photoelectron spectroscopy.

* Corresponding author at: Radioanalytical Chemistry Division, Bhabha Atomic Research Centre, Trombay, Mumbai 400085, India.

E-mail address: sumitk@barc.gov.in (S. Kumar).

1. Introduction

Deep geological disposal of high-level radioactive waste (HLW) is widely agreed upon as the solution for the long-term biospheric isolation of radiotoxic, long lived actinides, fission and activation products present in HLW [1]. The safety and performance analysis of the nuclear disposal facilities, therefore, require a comprehensive understanding of the mechanism of radionuclides interactions with mineral surfaces in the geochemical conditions of the disposal site [2–4].

In a deep underground repository, biotic as well as abiotic corrosion of metallic canisters/overpacks containing HLW may produce several iron oxides in the near-field areas of the radioactive source [5,6]. Magnetite ($\text{Fe}^{\text{II}}\text{Fe}^{\text{III}}_2\text{O}_4$), one of such oxides, exhibits reducing surfaces, causing immobilization of several mobile radionuclides [7,8]. Magnetite crystallizes in inverse spinel structure, Fe(II)/Fe(III) sharing octahedral (O_h) sites of the oxide (O^{2-}) FCC lattice while only Fe(III) populates the tetrahedral sites [7]. The presence of the Fe(II)/Fe(III) redox couple in O_h sites causes high electron conductivity through the magnetite lattice and thereby makes magnetite a redox-sensitive oxide. Naturally occurring magnetites are, however, ubiquitously substituted by divalent (Co, Ni, Mn etc.), trivalent (V, Cr, etc.) or tetravalent (Ti) transition elements in their lattice [9]. Literature studies investigating impurity atom distribution indicates substitution of Fe(II), Fe(III) or both Fe(II) and Fe(III) by the doped atoms [10,11]. Al-Rashdi et al. observed the substitution of octahedral Fe(III) by Mn(II) at low level of doping; increased Mn(II) doping replaces Fe(III) present in tetrahedral sites as well [11]. Higher Mn content in the solids results in the formation of higher oxidation states (III and IV) of Mn. This leads to the activation of additional redox couples (Mn(II)/Mn(III) and Fe(II)/Mn(III)) in magnetite lattice [9,12]. In a detailed investigation on the structural effect of Ti doping in magnetite nanoparticles [13], Ti(IV) was found replacing Fe(III) and the charge compensation was achieved by the conversion of Fe(III) to Fe(II) in the unit cell. These structural changes have been related to the physico-chemical changes in the reactivity of the doped magnetites [9, 14,15].

Liang et al. attributed increasing Pb(II) adsorption capacity with Mn doping to the variations in microstructure and physicochemical properties of the doped magnetite samples [9]. Latta et al. [16] argued the effect of Ti doping as controlling redox reactivity of titanomagnetite through changing bulk $\text{Fe}^{2+}/\text{Fe}^{3+}$ ratio. In reaction of U(VI) with titanium substituted magnetites ($\text{Fe}_{3-x}\text{Ti}_x\text{O}_4$), the presence of structural Ti ($x = 0.2\text{--}0.53$) causes the formation of U(IV) species that lack the bidentate $\text{U-O}_2\text{-U}$ bridges of uraninite (UO_2) forming on undoped magnetite surface [16]. Similar reduction and species were obtained in Np(V) reaction with titanomagnetite at low Np concentration [17]. X-ray absorption fine structure spectroscopy (XAFS) revealed a Np(IV) binding exclusively to the terminal Ti-O sites as opposed to Fe-O sites [17]. To the best of the authors' information, effect of Mn doping on actinides sorption on magnetite is absent in literature. Though less abundant than iron in environment, Mn exists as dopant as well as in form of its various oxides [18,19]. Strong sorption and speciation dependence of actinides on composition have been observed in case of manganese oxides [18]. A synchrotron-based micro X-ray fluorescence study observed plutonium (Pu(V)) being predominantly associated with manganese oxides ($\text{rancielite}; (\text{Ca}, \text{Mn}^{2+})_{0.4}\text{Mn}^{4+}\text{O}_2 \cdot 3\text{H}_2\text{O}$) and smectite clay but not with iron oxides (hematite; $\alpha\text{-Fe}_2\text{O}_3$) [20].

In the present study, Np(V) sorption and speciation have been investigated on magnetite (Fe_3O_4) and Mn-doped magnetites ($\text{Fe}_{3-x}\text{Mn}_x\text{O}_4$). Doping of Mn(II) was constrained to content below 12 wt % so as to isomorphously disperse Mn in the magnetite lattice and to avoid the formation of any new crystalline phase. Aims of the experiments were to explore (1) speciation of Np on Mn-doped magnetite vis-à-vis undoped magnetites and thereby, (2) if there existed, compared to Fe-O sites, any preference of sorbing Np toward Mn-O sites. Higher spectral resolution achieved with the High-energy resolution X-ray absorption near edge structure (HR-XANES) spectroscopy at Np M_5

absorption edge was employed to distinguish Np species forming on magnetites. The present study is important as the electronic structures of Mn and Fe are very different, they form oxides having different structural arrangement of cations [21], and they exhibit significantly different reactivity towards contaminants in the environment [20,22].

2. Material and methods

All sample preparations, manipulations and measurements were carried out in argon (Ar) or helium-filled glove boxes with < 0.1 ppmv O_2 . Mineral synthesis was carried out in anoxic condition under Ar flow. Experiments were carried out at room temperature using degassed (argon saturated) ultrapure water ($18.2 \text{ M}\Omega \text{ cm}$) and analytical grade chemicals (Sigma-Aldrich, Germany).

2.1. Magnetite synthesis and characterization

Magnetite particles (FMs) were synthesized by NaOH precipitation of Fe(II) solutions [23]. Briefly, 0.90 M Fe(II) ($\text{FeSO}_4 \cdot 7\text{H}_2\text{O}$) solution was prepared in pH ~ 1 HCl medium and heated to 90°C under constant stirring. Equal volumes of a solution containing 4.0 M NaOH and 0.9 M NaNO_3 were added dropwise to the heated Fe(II) solution over a period of ~ 5 h. Subsequently, the suspension was left for cooling under room temperature in anoxic condition. During the whole reaction sequence, flow of Ar gas through the precipitating solutions was ensured to prevent air oxidation of Fe(II) ions. Synthesized particles were separated by centrifugation at 5000 rpm for 5 min, washed with warm water three times and dried under the anaerobic atmosphere. Mn-doped (3–11 wt%; FM1–3) magnetites were synthesized by substituting the required amount of Fe(II) by Mn(II) ($\text{MnSO}_4 \cdot \text{H}_2\text{O}$) keeping the starting cation concentration the same (0.90 M).

The chemical composition of the synthesized magnetites was determined by dissolving ~ 0.05 g of magnetite in HCl medium followed by inductively coupled plasma - mass spectrometry (ICP-MS) measurements. Solid particles were characterized by recording x-ray diffraction (XRD) patterns, using a Bruker D8 Advance diffractometer equipped with a $\text{Cu K}\alpha$ radiation source and an energy-dispersive detector (Sol-X). A small suspension of the solids was dried on an air-tight low background sample holder to ensure anoxic conditions during measurements. DIFFRAC.EVA v. 3.1 program was used to analyse the XRD data. The specific surface area of the synthesized particles was measured by the Brunauer-Emmett-Teller (BET) method following N_2 adsorption/desorption at 77 K.

2.2. Sorption experiments

Sorption experiments were carried out in 15 mL polypropylene tubes. An aliquot ($\sim 50 \mu\text{L}$) of $0.013 \text{ M } ^{237}\text{Np(V)}$ solution (in 0.1 M HCl medium) was spiked into $3.00 (\pm 0.01) \text{ g L}^{-1}$ magnetite suspensions (0.01 M NaCl medium) to achieve a final Np(V) concentration of $2.1 (\pm 0.1) \times 10^{-5} \text{ M}$ in each sample. pHs of the suspensions were adjusted to ~ 7 employing slow addition of NaOH solution. The tubes were left for equilibration, with periodic shaking. After a period of 30 days, pHs of the suspensions were measured and the two phases were separated using centrifugation. The supernatant was mixed with 2% HNO_3 solution for ICP-MS based chemical analysis of dissolved Fe and Mn and for the determination of the left-over (aqueous) Np. After the experiment, tubes were washed with ultrapure water twice to softly remove the solid particles. Subsequently, 10 mL of 2% HNO_3 solution was contacted with the tubes over 24 h to check Np sorption on tube wall. Np sorption on the tube walls was found negligible.

2.3. XPS and SEM characterization of Np sorbed solid surfaces

To determine the oxidation state of Np present on the magnetite surface, X-ray photoelectron spectroscopic (XPS) measurements were

Table 1

Experimental conditions for the reaction of Np(V) with magnetite and Mn-doped magnetites.

Sample	Symbol	pH _f	N ₂ - based BET specific surface area (m ² g ⁻¹)	[Np (V)] _i , mol/L	[Np (V)] _f , mol/L	[Mn (aq)] _i , mol/L	[Mn (aq)] _f , mol/L
Magnetite (Fe ₃ O ₄)	FM0	7.08	12.3	2.1 × 10 ⁻⁵	5.9 × 10 ⁻⁸	—	—
3.6 wt% Mn-magnetite (Fe _{2.85} Mn _{0.15} O ₄)	FM1	7.16	13.2	2.0 × 10 ⁻⁵	4.0 × 10 ⁻⁸	3.5 × 10 ⁻⁵	3.1 × 10 ⁻⁵
5.5 wt% Mn-magnetite (Fe _{2.77} Mn _{0.23} O ₄)	FM2	7.05	11.9	2.1 × 10 ⁻⁵	7.4 × 10 ⁻⁸	4.5 × 10 ⁻⁵	4.5 × 10 ⁻⁵
10.9 wt% Mn-magnetite (Fe _{2.54} Mn _{0.46} O ₄)	FM3	7.06	15.6	2.1 × 10 ⁻⁵	4.5 × 10 ⁻⁸	13.8 × 10 ⁻⁵	13.2 × 10 ⁻⁵

pH_f represents the pH of the Np-equilibrated magnetite suspensions just before the supernatant-solids separation. Suspensions are having solids in 3.0 ± 0.1 g/L strength and 10 mL experimental volume of the suspensions. All equilibration experiments were carried out at room temperature and under Ar atmosphere. [Np(V)]_{i/f} denotes added and finally measured Np concentration in supernatant. [Mn(aq)]_{i/f} represents Mn concentration present in experimental supernatants before and after Np(V) contact. Uncertainties on the concentration data are estimated to be < ± 10%.

carried out with Np(V) contacted magnetite samples. Moist Np-magnetite samples were dried on indium foil under Ar atmosphere and mounted on a sample holder. Samples were transferred into the photoelectron spectrometer using an O-ring sealed vacuum transfer vessel. XPS measurements were carried out using a ULVAC-PHI Versa Probe II instrument equipped with a monochromatized Al K_α X-ray source (1486.7 eV) operated at 33 W source power. The spectrometer has a hemispherical capacitor analyzer and a detector consisting of a micro channel plate with 16 anodes. Calibration of the binding energy scale of the spectrometer was performed using well established binding energies of elemental lines of pure metals (surface cleaned by Ar ion beam sputtering, monochromatic Al K_α: Cu 2p_{3/2} at 932.62 eV, Au 4f_{1/2} at 83.96 eV). To evaluate the effect of sorbing Np on Fe and Mn oxidation states of magnetites, XPS measurements were also carried out for higher Mn doped magnetite samples and were compared with the corresponding Np(V) contacted samples.

Evolution of the morphology of magnetite particles upon interaction with Np in the sorption experiment was investigated using scanning electron microscopy (SEM). High resolution-SEM images of the magnetite samples were recorded with a FEI Quanta 650 FEG ESEM instrument.

2.4. X-ray absorption spectroscopic (XAS) measurements

Samples for XAS measurement were prepared similar to the sorption samples. After separation from the supernatant, Np(V) contacted magnetite particles were filled under Ar-atmosphere in doubly contained sample holders for Np L₃, Mn K and Np M₅ edge measurements. They were stored temporarily in an anaerobic chamber and brought to the beamline just before the measurement.

Np L₃-edge (17,610 eV) and Mn K-edge (6539 eV) XAS measurements were carried out for Np-contacted magnetite samples in fluorescence mode using a five element Ge solid state fluorescence detector (Canberra-Eurysis) at INE beamline, KIT synchrotron light source, Karlsruhe, Germany [24]. Gas filled ionization chambers were used for measuring the incident X-ray beam and the transmitted beam for energy calibration purpose. The monochromator, Ge(422) double-crystal setup, was calibrated using the first inflection point of the K-edge spectrum of an yttrium foil for Np L₃ edge measurements. For Mn K edge measurements, the monochromator was equipped with a pair of Si(111) crystals and an iron foil served for energy calibration purpose. Np M₅-edge (3664 eV) high-energy resolution X-ray absorption near edge structure (HR-XANES) measurements were carried for Np-contacted magnetites using a Johann type X-ray emission spectrometer installed at the ACT station of the CAT-ACT beamline, KIT synchrotron light source [25,26]. The incoming X-ray beam was monochromatized by a Si(111) double-crystal monochromator and HR-XANES spectra were acquired by following the intensity of the M_α emission (3261 eV) diffracted by five spherically bent Si(220) crystal analyzers (1 m bending radius) aligned at 81.92° Bragg angle (corresponding to the maximum of the normal emission line well above the M₅-edge). A single diode VITUS silicon drift

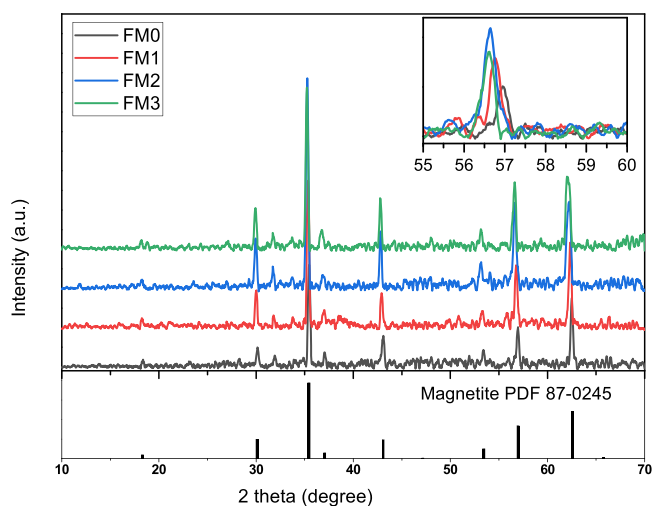


Fig. 1. X-ray diffraction pattern of the magnetite samples. FM0 refers to undoped magnetite while FM1 to FM3 refer to magnetites with increasing Mn doping (~ 4, 6 and 11 wt%). Inset picture highlights the shift in the diffraction peak at 2 theta value ~ 56°.

detector in a vertical Rowland geometry (diameter 1 m) was used to detect the crystal-scattered radiation. A gas tight box, enclosing the spectrometer and the sample, maintaining constant He atmosphere during the measurements was used to minimize intensity losses of impinging and emitted radiation due to scattering in the air atmosphere. The experimental energy resolution was found 1 eV by measuring the full width at half maximum of the elastically scattered incident beam.

K- and L₃-edge XAS spectra were analyzed using the ATHENA and ARTEMIS interfaces to the IFFEFIT suite of programs [27]. Analysis was carried out by extracting the extended X-ray absorption fine structure (EXAFS) spectra ($\chi(k)$) from the raw data, followed by its Fourier transform to frequency space which gives a spectrum (called in R-space) corresponding to the radial distribution of distances of neighboring atoms around the probed atom. The data in R-space was modeled using scattering paths from various Np (NpO₂) and Mn standards (Mn^{II}O, Mn^{III}₂O₃) [28–30]. For the scattering paths, phase and amplitude functions were generated using the Feff 8.4 software [31]. The amplitude reduction factor was set to 1.0 in the analysis. Uncertainties on the fitted parameters found in the modeling exercise have been listed in table S1. The fit quality was quantified by R_f factor [27], giving an idea on the deviation of modeled data from the experimental one. Analysis of Mn K-edge data were carried out by considering Mn substitution in Fe tetrahedral or octahedral site of magnetite lattice. HR-XANES spectra were processed using the PyMCA software [32]. Spectra were subsequently normalized to the white-line peak maximum.

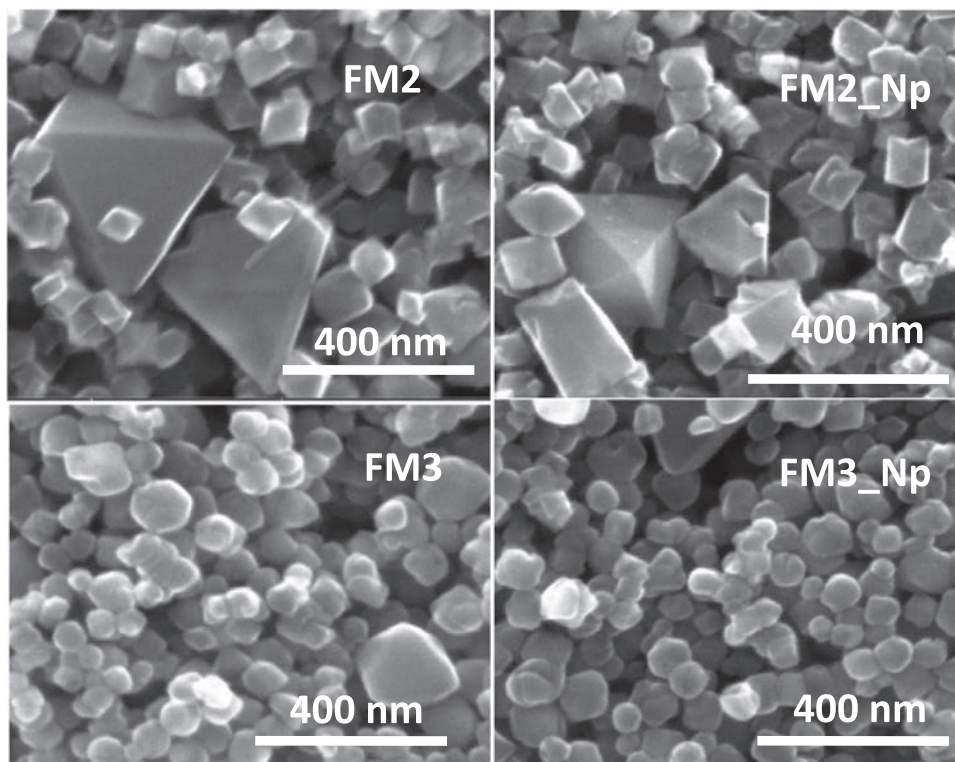


Fig. 2. Scanning electron micrographs of Mn doped magnetites (FM2, FM3) and their Np(V) contacted counterparts (FM2_Np, FM3_Np).

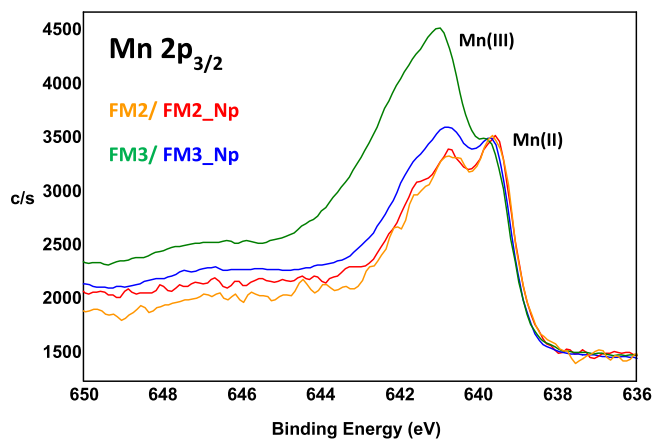


Fig. 3. XPS spectra (Mn $2p_{3/2}$ lines) of Mn-doped magnetites and their Np(V) contacted counterparts.

3. Results and discussion

3.1. Magnetites formation

Elemental composition, percentage of Mn doping and BET surface area of the magnetite (FM0) and Mn-doped magnetites (FM1–3) are given in Table 1. X-ray diffraction (XRD) pattern (Fig. 1) of the synthesized solids showed diffraction peaks identical to those of magnetite (JCPDS card no. 87-0245) and no trace of any other solid was observed. It further showed shifting of diffraction peaks to lower 2θ values (inset, Fig. 1) commensurate with increasing doping level of higher ionic radii species (substitution of Fe(II)/Fe(III) by Mn(II)) in the magnetite lattice [33].

3.2. Np(V) sorption on magnetites and characterization of sorbed solids

On equilibration, quantitative Np(V) sorption was achieved in all the magnetites suspensions (Table 1). Equilibrated pH of the suspensions was found to be 7.1 ± 0.1 . Mn solubility in the supernatant was found significant for all the magnetites and increased with doping level; however, there was a small decrease in Mn solubility on Np contact (Table 1). SEM images of the Np-sorbed magnetites (FM2/3_Np) vs. bare magnetites (FM2/3) are shown in Fig. 2. For all the doping level, the octahedral shape of the magnetite crystals was clearly visible; at the highest level of Mn doping (~ 11 wt%) rounding of the edges of the octahedra was observed. Particle morphology of magnetite crystals did not undergo any significant change on Np contact. The observation that rounding of the edges is related to Mn doping is validated with the similar finding seen for MnFe_2O_4 and $\text{Mn}_{1.8}\text{Fe}_{1.2}\text{O}_4$ solid oxides [34,12].

XPS and Mn K-edge XANES spectroscopy were carried out to follow possible change of Mn oxidation state on contact with Np(V). XPS, owing to ~ 2 nm depth sensitivity at Mn $2p_{3/2}$ line energy, probes the oxidation state change confined to few surface layers while XANES being sensitive to the bulk of the matrix (Mn K-edge energy 6.539 keV) delineates the oxidative changes occurring on the scale of the whole matrix. Fig. 3 plots Mn(II)-intensity normalized XPS spectra of Mn doped magnetite samples and their Np(V) contacted counterpart. On contact with Np(V), Mn(III) vs. Mn(II) signal for magnetite doped up to ~ 6 wt% (i.e., FM1 and FM2 samples) did not change. In FM3, enhanced surface presence of Mn(III) lowered on contact with Np(V). Possible reasoning for lowering of Mn(III) signal could be: 1) reduction of Np(V) by Mn(III)/Mn(IV) redox couple, 2) enhanced dissolution of Mn(III) from the surface, and 3) participation of Fe(II)/Mn(III) redox couple for the reduction of Np(V). In the first case, Mn(III) provides an electron to Np(V) and thereby oxidizes into Mn(IV). Signal of Mn(IV) ($2p_{3/2}$ binding energy 642.95 eV) [12] was not found in XPS of Np contacted FM3 sample. In this scenario application of Mn(III)/Mn(IV) redox couple is rejected. Enhanced solubility of Mn(III) on Np(V) contact can be ruled out as the enhanced solubility was not observed in the present study (Table 1). Np

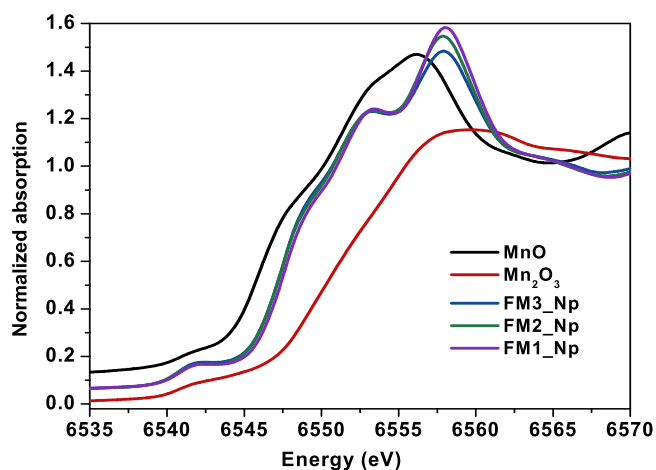


Fig. 4. Mn K edge XANES of Np-contacted magnetites and Mn standards. Spectra for the MnO and Np-contacted magnetites samples have been vertically shifted for better comparison of spectral features.

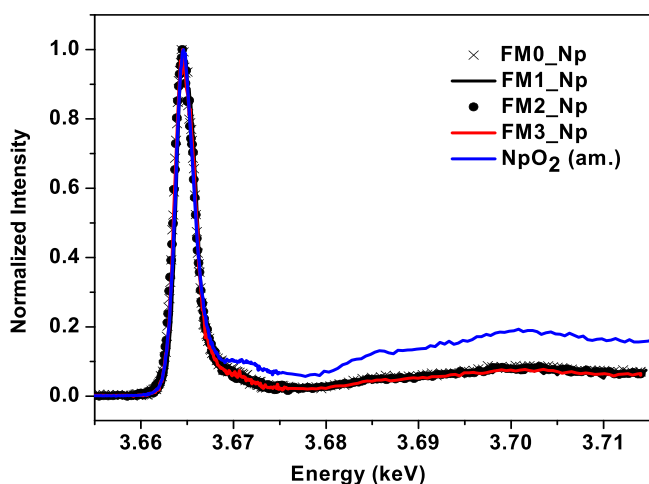


Fig. 5. Np M₅ absorption edge HR-XANES spectra of Np(V) contacted magnetites and Np(IV) oxide/hydroxide precipitate.

(V) reduction reaction with the redox couple Fe(II)/Mn(III) ($E^0 = 0.74$ V) [35], therefore seems responsible for the lowering of surface present Mn(III). Herein electron transfer from Fe(II) to Mn(III) will

enhance Mn(II) in its proportion with Mn(III). The presence of primary redox couple, Fe(II)/Fe(III) ($E^0 = 0.77$ V) [35], in magnetites and the observation that Fe(II)/Mn(III) participates only when Mn is present above 6 wt% points to the fact that a critical minimum concentration of Mn is required for Fe(II)/Mn(III) to play a role in the reduction of Np(V). Peng et al. [35] demonstrated the participation of Fe(II)/Fe(III) and Mn (II)/Mn(III) redox couples in the initial (< 70 min) and later (> 70 min) stages of methylene blue decomposition in neutral pH solution, respectively. Herein, however, in both stages of the catalytic performance of MnFe₂O₄ solid, the Fe(II)/Mn(III) redox couple accelerates the individual redox couples [35].

Mn K-edge XANES of Np(V)-contacted Mn-doped magnetites compared to that of standards (Mn^{II}O and Mn^{III}₂O₃), shown in Fig. 4, indicates (1) no significant differences in spectral features and hence similar distribution of Mn(II) and Mn(III) in the bulk of all the three Np (V)-contacted magnetite samples, and (2) leaning of XANES features of magnetite samples towards that of Mn(II) standard. Liang et al. [10] observed shifting of the Mn K-edge to higher energy values with increasing Mn content in the bare Mn-doped magnetite. This shift was attributed to an increase in average oxidation state of Mn in the solid (observed for MnO and Mn₂O₃ solids in the present study). Overlapping spectral features observed in the present study for all the three Np-contacted magnetites therefore attest to the overall dominance of Mn (II) in doped magnetites, either due to non-interaction of Mn with Np as in FM1/2_Np or when Mn(III) gets reduced by Np(V) as in FM3_Np sample.

3.3. Neptunium speciation on magnetites

Fig. 5 depicts Np M₅ absorption edge HR-XANES spectra of Np(V) contacted magnetite samples along with the spectrum of an amorphous Np(IV) oxide/hydroxide precipitate. For all FM solids, the white line spectral features overlay and closely match with resonances observed for Np^{IV}O₂ solid. This indicates Np presence on FM solids in + 4 oxidation state. HR-XANES, with capability to analyse fluorescence photon spectra with energy resolution better than the natural linewidth [36], has successively been employed to delineate the simultaneous existence of two species (CoO and Co nanoparticles) on carbon nanotube surface [37]. In view of this observation, the spectra in the present study, therefore, suggest the formation of a single speciation of Np (same or similar to NpO₂(am.)) on FM solids. Fig. S1 shows the Np 4f XPS peaks for Np(V) contacted FM2 and FM3 samples. 4f_{5/2} and 4f_{7/2} peaks overlay for these samples and these two peaks match values reported for NpO₂ solid (402.6, 414.3 eV, respectively) [38]. These evidences thus conclude the sorbed Np in a local structure very similar to NpO₂ solid.

Fourier transform (Fig. 6 [B]) of Np L₃ edge EXAFS spectra (Fig. 6

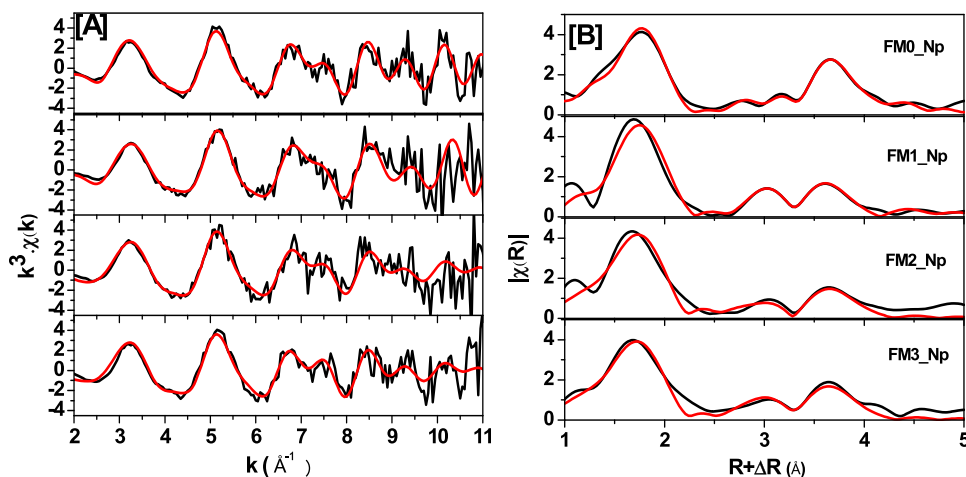


Fig. 6. [A] Np L₃ edge EXAFS spectra for Np(V) contacted magnetite samples labeled FM_xNp: x = 0–3, and [B] their Fourier transform.

[A]) contain peaks at ~ 1.7 , 3.0 and 3.6 Å (phase uncorrected). The higher distance peak was modeled with a Np - Np scattering path representing photoelectron wave scattering by surrounding Np atom found in the Np - O - Np bridging of NpO₂ solid. Modeling of the R-space data (Table S1) indicates the presence of 7–8 oxygen atoms at 2.33 Å. This radial distance matches the FCC unit cell of oxygen-octacoordinated Np (IV) confirming the formation of NpO₂ as the surface speciation of Np sorbed on magnetites/doped magnetites [39,40]. Furthermore, a coordination number < 1 for Np - Fe/Mn scattering path was found at ~ 3.41 Å. Owing to Z/Z + 1 character for the atomic numbers of Fe and Mn, it is not possible to differentiate between Fe and Mn in this fitting procedure. As there is higher uncertainty associated with coordination number [41], the presence of a Np - Fe/Mn scattering path simply indicates the sorption site of Np(V) on the solids before reduction to NpO₂(s).

To further confirm the sorption mechanism of Np(V) on magnetites, the Mn K - edge EXAFS spectrum for Np contacted FM3 sample was analyzed. Data was well modeled considering the structure of magnetite wherein Mn replaces the octahedral site Fe in magnetite lattice. Simulation of the data (Fig. S2 and Table S2) changed minimally (reduced chi-squared changed from 3.09 to 3.38) by including Mn - Np scattering path. The Hamilton test (based on R-factor of the fitting process) for the model with Mn - Np path, however, indicates 95% chances that there is improvement of fit on considering this scattering shell (Table S3) [41]. Fitting data for the Mn - Np shell match well with that for Np - Mn/Fe shell found in Np L₃ edge data fitting. These results, thus, conclude to the formation of a single species of sorbing Np(V), i.e., nano-particulate Np^{IV}O₂ (solid), on magnetite as well as Mn-doped magnetites. Mn-O sites show some preference for sorbing Np(V) compared to Fe-O sites but the presence of Mn in the magnetite lattice does not change the surface speciation of sorbed Np. Mn participates through Fe(II)/Mn(III) redox couple in reducing sorbed Np(V) and its participation becomes significant only when the doped-magnetite contains a critical minimum concentration (> 6 wt%) of Mn. In light of this study, the role of Mn in the surface speciation of Np is significant only at higher level of Mn doping.

4. Summary and conclusion

The present study investigates spectroscopically the role of manganese (Mn) present as impurity in magnetite lattice in the sorption mechanism of neptunium. Homogenous distribution of Mn in magnetite was achieved by synthesizing magnetites with Mn doping over 3–12 wt %. X - ray diffraction pattern, however, revealed the shifting of diffraction peaks to lower 2 theta values in agreement with Fe(II)/Fe(III) replacement by Mn(II). Quantitative sorption of neptunium, Np(V), was observed on both undoped and doped magnetites in neutral pH condition. Np(V) sorption suppressed Mn solubility in case of magnetite with highest Mn doping. In a surface sensitive investigation of Np(V) contacted magnetites by X-ray photoelectron spectroscopy, Mn(II) changing to Mn(III) was observed on interaction with Np(V), though the effect is pronounced only when the doping is above 6 wt%. Nanoparticulate neptunium(IV) oxide surface speciation was indicated in Np M₅ edge HR-XANES measurement of Np(V) sorbed on Mn-doped as well as undoped magnetites and was confirmed using analysis of Np L₃ edge EXAFS data. These observations conclude that Mn-O site does show preference for sorbing Np(V) vis-à-vis Fe-O site but participates only through Fe(II)/Mn(III) redox couple in deciding Np(V) surface speciation on magnetites. This study, thus, shows another end of impurity role wherein it does not affect the surface speciation coordinatively but only through its redox reaction.

CRedit authorship contribution statement

Sumit Kumar: Conceptualization, Data curation, Methodology, Software, Writing - original draft, Writing - review & editing. **Jorg**

Rothe: Conceptualization, Data curation, Writing - review & editing, Project administration. **Nicolas Finck:** Data curation, Writing - review & editing. **Tonya Vitova:** Data curation **Aaron Beck:** Data curation. **Kathy Dardenne:** Data curation. **Dieter Schild:** Data curation. **Horst Geckeis:** Project administration, Resources, Supervision.

Declaration of Competing Interest

The authors declare that they have no known competing financial interests or personal relationships that could have appeared to influence the work reported in this paper.

Acknowledgements

Sumit Kumar acknowledges Alexander von Humboldt Foundation (ref no. IND - 1186791 - HFST-P) and Bhabha Atomic Research Centre, Mumbai, India for making possible this work during his postdoctoral fellowship at KIT-INE. Authors express gratitude to Dr. David Fellhauer for providing the neptunium solution, Ms. Tanja Kisely for carrying out the N₂-BET analysis of the solids, Mr. F. Geyer and Ms. C. Walschburger for ICP-MS measurements. Authors acknowledge the KIT synchrotron light source and the Institute for Beam Physics and Technology (IBPT) for operation of the Karlsruhe Research Accelerator (KARA).

Supporting Information

XPS spectra and EXAFS fitting result of Np L₃ edge spectra for Np(V) contacted undoped and doped magnetites (FM0-3_Np), EXAFS fitting result of Mn K-edge spectra for Np(V) contacted magnetites (FM3_Np).

References

- [1] Assessment of disposal options for DOE-managed high-level radioactive waste and spent nuclear fuel, Department of Energy (US DOE) Report, 2014.
- [2] J. Wang, L. Chen, R. Su, X. Zhao, The Beishan underground research laboratory for geological disposal of high-level radioactive waste in China: planning, site selection, site characterization and in situ tests, *J. Rock. Mech. Geotech. Eng.* 10 (2018) 411–435.
- [3] H. Geckeis, J. Lützenkirchen, R. Polly, T. Rabung, M. Schmidt, Mineral-water interface reactions of actinides, *Chem. Rev.* 113 (2013) 1016–1062.
- [4] B. Ma, L. Charlet, A. Fernandez-Martinez, M. Kang, B. Made, A review of the retention mechanisms of redox-sensitive radionuclides in multi-barrier systems, *Appl. Geochem.* 100 (2019) 414–431.
- [5] M.L. Schlegel, C. Bataillon, K. Benhamida, C. Blanc, D. Menut, J.L. Lacour, Metal corrosion and argillite transformation at the water-saturated, high-temperature iron-clay interface: a microscopic scale study, *Appl. Geochem.* 23 (2008) 2619–2633.
- [6] M. Etique, A. Romaine, I. Bihannic, R. Gley, C. Carteret, M. Abdelmoula, C. Ruby, M. Jeannin, R. Sabot, P. Refait, F.P. A. Jorand, Abiotically or Microbially mediated transformation of magnetite by sulphide species: the unforeseen role of nitrate-reducing bacteria, *Corr. Sci.* 142 (2018) 31–44.
- [7] M. Usman, J.M. Byrne, A. Chaudhary, S. Orsetti, K. Hanna, C. Ruby, A. Kappler, S. B. Haderlein, Magnetite and green rust: synthesis, properties, and environmental applications of mixed-valent iron minerals, *Chem. Rev.* 118 (2018) 3251–3304.
- [8] D. Li, D.I. Kaplan, Sorption coefficients and molecular mechanisms of Pu, U, Np, Am and Tc to Fe (hydr)oxides: a review, *J. Hazard. Mater.* 243 (2012) 1–18.
- [9] X. Liang, Z. He, G. Wei, P. Liu, Y. Zhong, W. Tan, P. Du, J. Zhu, H. He, J. Zhang, The distinct effects of Mn substitution on the reactivity of magnetite in heterogeneous Fenton reaction and Pb(II) adsorption, *J. Colloid Interface Sci.* 426 (2014) 181–189.
- [10] X. Liang, Yuan-Hong Zhong, S. Zhu, H. He, P. Yuan, J. Zhu, Z. Jiang, The valence and site occupancy of substituting metals in magnetite spinel structure Fe_{3-x}M_xO₄ (M = Cr, Mn, Co and Ni) and their influence on thermal stability: an XANES and TG-DSC investigation, *Solid State Sci.* 15 (2013) 115–122.
- [11] K.S. Al-Rashdi, H.M. Widatallah, F. Al Má Mari, O. Cespedes, M. Elzain, A. Al-Rawas, A. Gismelseed, A. Yousif, Structural and Mossbauer studies of nanocrystalline Mn²⁺ doped Fe₃O₄ particles, *Hyperfine Interact.* 239 (2018) 3.
- [12] Gui-Xiang Huang, Chu-Ya Wang, Chaun-Wang Yang, Pu-Can Guo, Han-Qing Yu, Degradation of Bisphenol A by peroxymonosulfate catalytically activated with

- Mn_{1.8}Fe_{1.2}O₄ nanospheres: synergism between Mn and Fe, *Environ. Sci. Technol.* 51 (2017) 12611–12618.
- [13] C.I. Pearce, O. Qafoku, J. Liu, E. Arenholz, S.M. Heald, R.K. Kukkadapu, C. A. Gorski, C.M.B. Henderson, K.M. Rosso, Synthesis and properties of titanomagnetite (Fe_{3-x}Ti_xO₄) nanoparticles: a tuneable solid-state Fe(II)/Fe(III) redox system, *J. Colloid Interface Sci.* 387 (2012) 24–38.
- [14] S. Garcia, S. Sardar, S. Maldonado, V. Garcia, C. Tamez, J.G. Parsons, Study of As (III) and As(V) oxyanion adsorption onto single and mixed ferrite and hausmannite nanomaterials, *Microchem. J.* 117 (2014) 52–60.
- [15] M.J. O'Hara, J.C. Carter, C.L. Warner, M.G. Warner, R.S. Addleman, Magnetic iron oxide and manganese-doped iron oxide nanoparticles for the collection of alpha-emitting radionuclides from aqueous solutions, *RSC Adv.* 6 (2016) 105239–105251.
- [16] D.E. Latta, C.I. Pearce, K.M. Rosso, K.M. Kemner, M.I. Boyanov, Reaction of U^{VI} with titanium-substituted magnetite: influence of Ti on U^{IV} speciation, *Environ. Sci. Technol.* 47 (2013) 4121–4130.
- [17] E.M. Wylie, D.T. Olive, B.A. Powell, Effects of titanium doping in titanomagnetite on neptunium sorption and speciation, *Environ. Sci. Technol.* 50 (2016) 1853–1858.
- [18] A.E. Hixon, B.A. Powell, Plutonium environmental chemistry: mechanisms for the surface-mediated reduction of Pu(V/VI), *Environ. Sci.: Process. Impacts* 201 (2018) 1306–1322.
- [19] Y.J. Hu, L.K. Schwaiger, C.H. Booth, R.K. Kukkadapu, E. Cristiano, D. Kaplan, H. Nitsche, Molecular interactions of plutonium(VI) with synthetic manganese-substituted goethite, *Radiochim. Acta* 98 (2010) 655–663.
- [20] M.C. Duff, D.B. Hunter, I.R. Triay, P.M. Bertsch, D.T. Reed, S.R. Sutton, G. Shear-McCarthy, J. Kitten, P. Eng, S.J. Chipera, D.T. Vaniman, Mineral associations and average oxidation states of sorbed Pu on Tuff, *Environ. Sci. Technol.* 33 (1999) 2163–2169.
- [21] A.R. West, *Solid state chemistry and its applications*. Chapter 3, John Wiley & Sons, Ltd., United Kingdom, 2014.
- [22] R.D. Silva, Actinide environmental chemistry, *Radiochim. Acta* 70 (1995) 377–396.
- [23] R.M. Cornell, U. Schwertmann, *The Iron Oxides: Structure, Properties, Reactions, Occurrences and Uses*, Wiley, 2006.
- [24] J. Rothe, S. Butorin, K. Dardenne, M.A. Denecke, B. Kienzler, M. Loble, V. Metz, A. Seiber, M. Steppert, T. Vitova, C. Walthers, H. Geckeis, The INE beamline for actinide science at ANKA, *Rev. Sci. Instrum.* 83 (2012) 043105–043115.
- [25] A. Zimina, K. Dardenne, M.A. Denecke, D.E. Doronkin, E. Huttel, H. Lichtenberg, S. Mangold, T. Pruessmann, J. Rothe, T. Spangenberg, R. Steininger, T. Vitova, H. Geckeis, J.D. Grunwaldt, CAT-ACT-A new highly versatile x-ray spectroscopy beamline for catalysis and radionuclide science at the KIT synchrotron light facility ANKA, *Rev. Sci. Instrum.* 88 (2017) 113113–113125.
- [26] I. Pidchenko, K.O. Kvashnina, T. Yokosawa, N. Finck, S. Bahl, D. Schild, R. Polly, E. Bohnert, A. Rossberg, J. Gottlicher, K. Dardenne, J. Rothe, T. Schafer, H. Geckeis, T. Vitova, Uranium redox transformations after U(VI) coprecipitation with magnetite nanoparticles, *Environ. Sci. Technol.* 51 (2017) 2217–2225.
- [27] B. Ravel, M. Newville, ATHENA, ARTEMIS, HEPHAESTUS: data analysis for X-ray absorption spectroscopy using IFEFFIT, *J. Synchrotron Radiat.* 12 (2005) 537–541.
- [28] NpO₂ Crystal Structure, Pauling File id: sd_0451124, Pauling File in Inorganic Solid Phases, Springer Materials (Online Database), Springer, Heidelberg, 2016 (edition), https://materials.springer.com/isp/crystallographic/docs/sd_0451124.
- [29] R.E.G. Pacalo, E.K. Graham, Pressure and temperature dependence of the elastic properties of synthetic MnO, *Phys. Chem. Miner.* 18 (1991) 69–80.
- [30] S. Geller, Structures of α-Mn₂O₃, (Mn_{0.98}Fe_{0.017})₂O₃ and (Mn_{0.37}Fe_{0.62})₂O₃ and relation to magnetic ordering, *Acta Cryst. B* 27 (1971) 821–828.
- [31] A.L. Ankudinov, B. Ravel, J.J. Rehr, S.D. Conradson, Real-space multiple-scattering calculation and interpretation of x-ray-absorption near-edge structure, *Phys. Rev. B: Condens. Mater. Phys.* 58 (1998) 7565–7576.
- [32] V.A. Solé, E. Papillon, M. Cotte, Ph. Walter, J. Susini, A multiplatform code for the analysis of energy-dispersive X-ray fluorescence spectra, *Spectrochim. Acta Part B* 62 (2007) 63–68.
- [33] F.L. Deepak, M. Banobre-López, E. Carbo-Argibay, M. Fatima Cerqueira, Y. Pineiro-Redondo, J. Rivas, C.M. Thompson, S. Kamali, C. Rodriguez-Abreu, K. Kovnir, Y.V. Kolenko, A systematic study of the structural and magnetic properties of Mn, Co, and Ni-doped Colloidal magnetite nanoparticles, *J. Phys. Chem. C* 119 (2015) 11947–11957.
- [34] L. Xy, L. Jy, D. Sheng, L. Hz, Spinel-type manganese ferrite (MnFe₂O₄) microspheres: a novel affinity probe for selective and fast enrichment of phosphopeptides, *Talanta* 166 (2017) 36–45.
- [35] X. Peng, J. Qu, S. Tian, Y. Ding, X. Hai, B. Jiang, M. Wu, J. Qui, Green fabrication of magnetic recoverable graphene/MnFe₂O₄ hybrids for efficient decomposition of methylene blue and the Mn/Fe redox synergetic mechanism, *Rsc Adv.* 6 (2016), 104549 – 104549.
- [36] K. Hamalainen, D.P. Siddons, J.B. Hastings, L.E. Berman, Elimination of the inner-shell lifetime broadening in x-ray-absorption spectroscopy, *Phys. Rev. Lett.* 67 (1991) 2850–2853.
- [37] B. Liu, M.M. van Schooneveld, Yi-Tao Cui, J. Miyawaki, Y. Harada, T. O. Eschemann, K.P. de Jong, M.U. Delgado-Jaime, F.M.F. de Groot, In-situ 2p3d resonant inelastic X-ray scattering tracing cobalt nanoparticle reduction, *J. Phys. Chem. C* 121 (2017) 17450–17456.
- [38] Y.A. Teterin, Yu Teterin, K.E. Ivanov, M.V. Ryzhkov, K.I. Maslakov, S.N. Kalmykov, V.G. Petrov, D.A. Enina, X-ray photoelectron spectra structure and chemical bond nature in NpO₂, *Phys. Rev. B* 89 (2014), 035102.
- [39] K. Nakata, S. Nagasaki, S. Tanaka, Y. Sakamoto, T. Tanaka, H. Ogawa, Sorption and reduction of neptunium(V) on the surface of iron oxides, *Radiochim. Acta* 90 (2002) 665–669.
- [40] K. Nakata, S. Nagasaki, S. Tanaka, Y. Sakamoto, T. Tanaka, H. Ogawa, Reduction rate of neptunium(V) in heterogeneous solution with magnetite, *Radiochim. Acta* 92 (2004) 145–150.
- [41] S. Calvin, *XAFS for Everyone*, CRC Press, 2013.

Repository KITopen

Dies ist ein Postprint/begutachtetes Manuskript.

Empfohlene Zitierung:

Kumar, S.; Rothe, J.; Finck, N.; Vitova, T.; Dardenne, K.; Beck, A.; Schild, D.; Geckeis, H. [Effect of manganese on the speciation of neptunium\(V\) on manganese doped magnetites](#). 2022. Colloids and surfaces / A, 635.
doi: [10.5445/IR/1000141314](https://doi.org/10.5445/IR/1000141314)

Zitierung der Originalveröffentlichung:

Kumar, S.; Rothe, J.; Finck, N.; Vitova, T.; Dardenne, K.; Beck, A.; Schild, D.; Geckeis, H. [Effect of manganese on the speciation of neptunium\(V\) on manganese doped magnetites](#). 2022. Colloids and surfaces / A, 635, Article no: 128105.
doi: [10.1016/j.colsurfa.2021.128105](https://doi.org/10.1016/j.colsurfa.2021.128105)

Lizenzinformationen: [CC BY-NC-ND 4.0](#)